Blue-Green Systems

Blue-Green Systems Vol 7 No 2, 468 doi: 10.2166/bgs.2025.010

Risk-based design of grass swales: assessing the impact of soil hydraulic conductivity on swale overflow mitigation

Ivan Mantilla[a,*], Tone Merete Muthanna[b], Jiri Marsalek[a] and Maria Viklander[a]

[a] Department of Civil, Environmental and Natural Resources Engineering, Luleå University of Technology, 971 87 Luleå, Sweden
[b] Department of Civil and Environmental Engineering, Norwegian University of Science and Technology (NTNU), N-7491 Trondheim, Norway
*Corresponding author. E-mail: ivan.mantilla@ltu.se

IM, 0000-0002-4982-6060

ABSTRACT

To assess the reliability of green stormwater infrastructure (GSI), including grass swales, it is required to characterize the frequency of system failures. This involves identifying the conditions when the system operates in failure mode, potentially causing downstream flooding. The study utilized three 23-year meteorological time series from three Swedish locations, characterized by frontal, convective, or orographic rainfall events. These time series served as inputs for the simulation of runoff flows using the SWMM model, representing the physical characteristics of a grass swale (GS) located in Luleå, Sweden. Results showed a trend of reduced overflow occurrences and flood risks at higher *ksat* values of 25 and 31 mm/h. Exceedance curves indicated that *ksat* values of 2 or 4 mm/h resulted in the swale operating in failure mode 100% of the time. A minimum *ksat* of 31 mm/h was required to achieve acceptable operation for more than 50% of the time in Gothenburg and Luleå. Östersund was the only location where the studied GS did not operate in failure mode under a high *ksat* of 31 mm/h. Local climate – especially rainfall distribution and frequency – sets performance thresholds and underscores the need to integrate technical performance with flood risk management in GSI design.

Key words: failure operation, grass swales, overflow events, risk-based swale design, saturated hydraulic conductivity, stormwater management

HIGHLIGHTS

- Native soils with 2–4 mm/h *ksat* were found unsuitable for grass swales implementation.
- Infiltration rates of 2–4 mm/h resulted in 100% failure mode operation across all sites.
- In Östersund, under a *ksat* of 31 mm/h was achieved 100% of acceptable operation.
- A location with oceanic climates exhibited higher overflow risks.
- Local rainfall patterns drive performance thresholds, necessitating climate-specific swale design.

GRAPHICAL ABSTRACT

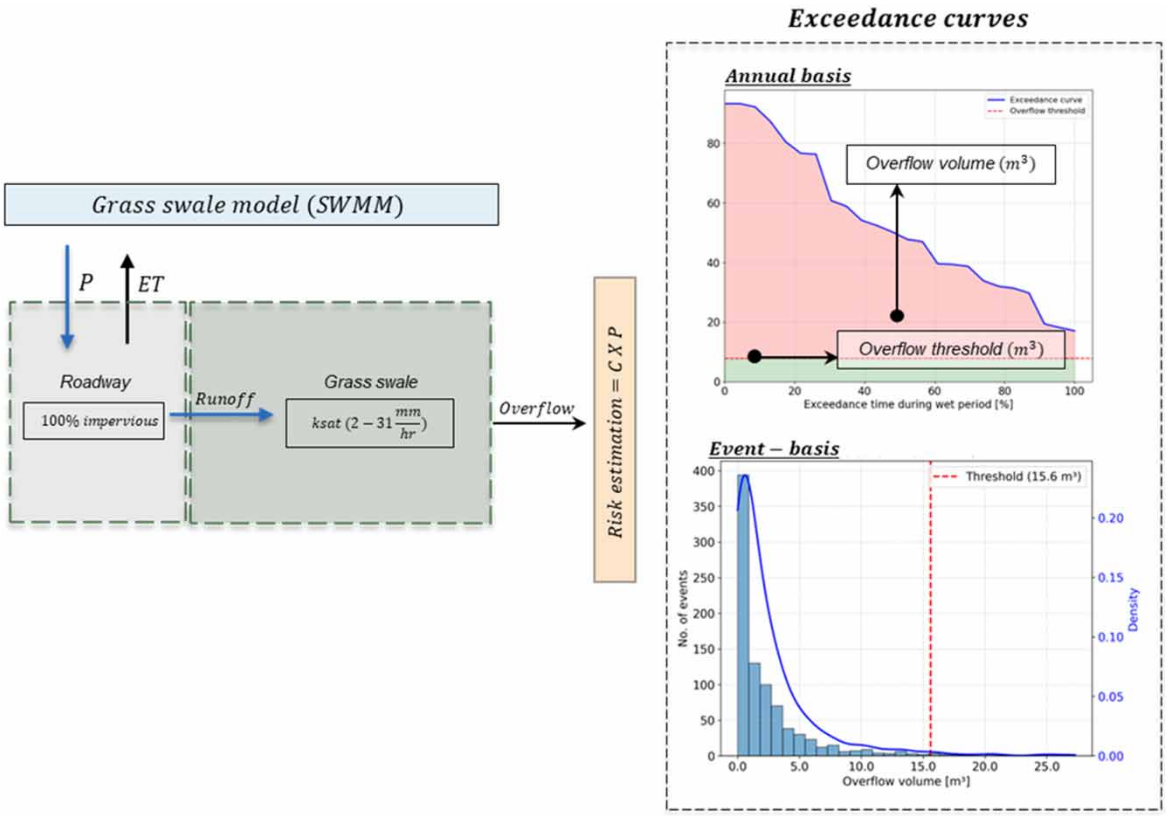

1. INTRODUCTION

Urban flood damages have risen in recent decades and are projected to further increase due to more frequent heavy rainfalls caused by climate change in some world regions (UNEP 2023). The growing risk of pluvial flooding highlights the need to enhance urban drainage resilience with drainage systems that can be adaptable to, and recoverable under, uncertain future conditions (Weathers *et al.* 2023). This is the result of predicted shifts in climate trends that create uncertainty in the capacity of urban drainage systems needed to maintain service levels (Tirpak *et al.* 2021a). In response, cities are implementing green stormwater infrastructure (GSI) to mimic pre-development hydrology by enhancing infiltration and evapotranspiration (ET) and thereby reducing runoff flow volumes and flood risks (Ballard *et al.* 2015). As cities aim to implement more resilient stormwater management infrastructure under changing climate conditions, a well-defined understanding of the acceptable risk associated with GSI design – targeting smaller, more frequent events – is essential (Lewellyn & Wadzuk 2019).

GSI has proved to be effective for flood risk management by reducing runoff flows and volumes (Deletic & Fletcher 2006; Fletcher *et al.* 2013). Among GSI facilities, grass swales are an effective option for managing road runoff because their linear layout fits the landscape and provides the benefits of stormwater conveyance, control, and treatment used for attenuating highway runoff toxicity before reaching receiving waters (Leroy *et al.* 2016). Traditionally, the prevention of urban floods during infrequent rain events has been described as a peak-flow control approach (Ballard *et al.* 2015). GSI design guidelines applied to a variety of geographic scales define permissible flow rates justified by (1) downstream drainage network capacities to prevent urban floods and (2) preservation of pre-development flow rates to prevent stream channel erosion (Brown *et al.* 2010). Indeed, stormwater flow reduction targets are usually defined as a metric for evaluating the performance of GSI facilities (delays of 80–90% of annual runoff volumes) and are usually associated with specific design storms (MDE 2009). However, there is a lack of consistency in evaluating the performance of GSI facilities due to the spatial and temporal variability of factors influencing their effectiveness, including local climatic conditions (Sage *et al.* 2015).

In Sweden, a survey of 26 biofilter cells revealed that at least 40% of the facilities lacked sufficient capacity to retain daily rainfall events and/or the design rainfall, indicating that water retention objectives were not met because of inadequate design or insufficient maintenance (Beryani *et al.* 2021). The evaluation of these facilities, based on design and maintenance indicators, identified issues such as concentrated flow paths, observed standing water, soil crusting and compaction, and evidence of erosion and/or clogging in the soil media. Under a changing climate, the capacity of existing GSI will likely be exceeded more frequently (Sohn *et al.* 2020). Adapting GSI to climate change requires not only upgrading physical infrastructure but also diligent maintenance to reduce flood risk during extreme events (Bahrami *et al.* 2024). For instance, Weathers *et al.* (2023) estimated a significant increase in biofilter cell overflow in the southern United States, ranging from 67 to 71%, under the projected rainfall intensities. Hathaway *et al.* (2014) found that the depth of ponding on the bioretention surface in North Carolina would need to be increased by 15.5–31 cm under the climate change scenario corresponding to the Representative Concentration Pathway (RCP) 4.5 to limit overflow volumes. While retrofits of existing GSI designs can reduce untreated surface overflows, attention must be directed to determining risk tolerance when assessing options to ensure bioretention effectiveness in future climate conditions (Tirpak *et al.* 2021b).

Flood risk management has attracted attention during recent decades, facilitating the selection of optimal strategies for risk reduction (Mens *et al.* 2011). Traditionally, flood risk assessments are based on the likelihood of system failure and the potential damages associated with that failure (Vorogushyn *et al.* 2018). These approaches are well-established for larger flood management systems but are rarely used to evaluate the effectiveness of GSI in reducing flood risk (Lewellyn & Wadzuk 2019). In earlier decades, engineers and planners defined acceptable levels of risk by using design storms; however, awareness of the linkage between the design criteria and risk has eroded over time (Hathaway *et al.* 2024). Adopting strategies with adaptive capacity in GSI could potentially reduce risk by decreasing the likelihood of system failure and the resulting damages (Lewellyn *et al.* 2016). For instance, the three-step approach (3SA) is a framework that helps reduce flood risk by integrating prevention, mitigation, and response strategies (Lindholm *et al.* 2008). This selection is based on varying rainfall magnitudes and event return periods, aiming to infiltrate smaller events, detain larger ones, and safely convey more severe events (Paus 2018). However, designing GSI according to this philosophy requires robust quantification of these solutions, which involves evaluating their performance under failure conditions (Pons *et al.* 2022a, b). There is a need to anticipate malfunctions and enhance the performance of GSI in the long term by characterizing periods with operational failures (Bahrami *et al.* 2024).

General design considerations for grass swales involve selecting physical attributes such as bottom width (e.g., 0.5–2.0 m), longitudinal slope (0.5–6%), side slope (maximum 1:3), and maximum depth (400–600 mm) (Ballard *et al.* 2015). Ekka *et al.* (2024) found that, to optimize swale function, designers should maximize swale length to the greatest extent practicable – especially when swales receive inflow from end-of-pipe systems draining roadway surfaces. While grassed swales are effective in reducing runoff volumes and improving water quality, introducing concentrated infiltration adjacent to pavements can raise subsurface moisture in the subgrade and fill, with three common failure modes: (1) pavement distress (cracking, rutting, potholing) from base-course saturation, (2) washouts of fines from beneath the pavement, and (3) embankment or roadside slope instability due to elevated pore pressures (MPCA 2005).

Moreover, saturated hydraulic conductivity (*ksat*) is a critical parameter for the design and post-construction performance of grass swales (Ebrahimian *et al.* 2020). Ahmed *et al.* (2015) conducted 722 infiltration measurements in five grass swales and reported large variations in *ksat*, with geometric means ranging from 7.5 to 390 mm/h – a relatively narrow span given the diversity of soil textures. Mantilla *et al.* (2025) evaluated the temporal and spatial variability of grass swale (GS) infiltration rates and found mean values ranging from 13 mm/h at the swale bottom to 98 mm/h on the right slope, along with a 52% decrease in infiltration rates between 2022 and 2024. Kanso *et al.* (2018) determined that four to eight infiltration measurements – on grass swales 32–50 m in length – are required to obtain a representative average *ksat* with an uncertainty of a factor of two or less. Furthermore, there is a need to identify the optimum GSI design to reduce flood risk in downstream urban areas, which involves a trade-off between surface storage and soil infiltration capacity (Winston *et al.* 2016).

The objective of this study is to determine how the selected physical design parameters of native soils, in which a GS is implemented, such as saturated hydraulic conductivity (*ksat*), contribute to reducing flood risk in urban areas. The study provides an understanding of the duration during which a GS operates within an acceptable performance threshold and quantifies the risk associated with failure mode operation. To achieve this, an evaluation of the *ksat* required to mitigate flood risk in urban areas is presented by examining the relationship between the overflow volume and various *ksat* values. Exceedance curves are presented to advance the understanding of the periods when grass swales operate above an acceptable threshold, and how rainfall patterns influence the occurrence of overflow events.

2. DATA COLLECTION AND METHODS

2.1. Data collection and study site descriptions

Climate data from January 1997 to December 2019 were retrieved from the national meteorological network operated by the Swedish Meteorological and Hydrological Institute (SMHI). Three urban locations across Sweden – Gothenburg, Luleå, and Östersund – were selected for the analysis based on the mechanisms of local rainfall generation. Gothenburg, Luleå, and Östersund exhibit distinct precipitation patterns influenced by their geographical locations and climatic conditions (Johansson & Chen 2003). Gothenburg, with a mean annual precipitation of 893 mm, experiences an oceanic climate (Cfb) (Köppen & Geiger 1936), in which rainfall is evenly distributed throughout the year (refer to Table 1). The wettest months are October and November, with a mean monthly precipitation of 92 and 84 mm, respectively (refer to Supplementary Figure S1(a)). Luleå, located in northern Sweden, has a subarctic climate (Dfc) (Köppen & Geiger 1936), and on average receives about 490 mm of precipitation annually. Rainfall mainly occurs between May and September, with the wettest months being July and August, with a mean precipitation of 70 and 67 mm, respectively. Östersund, situated near the Scandinavian Mountain range, experiences a subarctic climate (Dfc) with annual precipitation of around 539 mm. July and August are the wettest months, receiving 87 and 74 mm of rainfall, respectively (refer to Supplementary Figure S1(a)).

The analysis considers only the months when all precipitation occurs in the form of rainfall, defined as the periods with air temperatures >0 °C (Rossman & Huber 2016). Climate data consist of observed daily maximum and minimum temperatures (°C), 15-min precipitation (mm), daily wind speed (km/h), and daily relative humidity (%). These parameters were used to estimate ET for each urban area using the Penman–Monteith method. Analysis of precipitation records comprised identification of rainy days, defined as the days with precipitation depths greater than 1.0 mm, and of rain events defined as periods of rainfall separated by dry interevent times equal to or larger than 6 h (Hernebring 2006).

In addition, the data collection included observed inflow and outflow rates for the model calibration. These parameters were obtained by using a controlled irrigation system designed to simulate runoff flows from a roadway adjacent to the grassed swale and upstream areas according to Mantilla *et al.* (2024) (refer to Supplementary Figure S2(a)). Outflow rates were measured using a 120° V-notch weir at the swale downstream end, with water levels continuously recorded by a pressure transducer, and were derived from the Kindsvater-Carter formula (refer to Equation (1)) (Kindsvater & Carter 1957).

$$Q = \left(C_d \cdot \frac{8}{15} \cdot \tan(\theta/2)\,(2g)^{0.5} \cdot H^{2.5} \right) * 1,000 \tag{1}$$

Table 1 | Main climatic characteristics of urban study areas for the period of 1997–2019

Parameter	Urban areas: Gothenburg	Luleå	Östersund
MAP[a] (mm)	893	490	539
ADP[b] (days)	122	89	98
MMP[c] (mm)	74	41	45
Mean annual temperature (°C)	9.2	2.9	4.0
MPET[d] (mm/month)	41.0	47.1	47.3
AWD[e] (days)	30.3	78.7	70.6
Minimum winter temperature (°C)	−10.8	−41	−34
ASD[f] (days)	162.7	108	103.9
Climate classification[g]	Cfb	Dfc	Dfc
Meteorological station[h]	Gothenburg A	Älvsbyn A	Hunge A

[a]MAP is the mean annual precipitation.
[b]ADP is the average number of annual days with precipitation >1 mm.
[c]MMP is the mean monthly precipitation.
[d]MPET is the mean daily evapotranspiration (mm/day).
[e]AWD is the annual number of winter days with air temperature T < 0 °C (days).
[f]ASD is the annual number of days with T > 10 °C (days).
[g]Climatic classifications according to Köppen & Geiger (1936).
[h]Station from the national meteorological network operated by SMHI.

where Q is the flow rate (L/s), C_d is a non-dimensional discharge coefficient, θ is the angle of the V-notch, g is the gravitational acceleration, and H is the head over the weir. Discharge coefficients were adopted from International Standard Organization (2017), with a value of 0.595 for the 120° (WO scenario). Ground level was lowered downstream of the weir to maintain free flow conditions and prevent backwater effects. During irrigation experiments, the swale was outfitted with five water content reflectometers installed every 5 m along the swale bottom to monitor volumetric water content (VWC) and soil temperature (ST). Additionally, a 50-cm soil-profile probe was used to measure VWC, ST, soil permittivity (P), and electrical conductivity (EC) at different depths (10, 20, 30, 40, and 50 cm). Inflow rates were based on the design block rainfall approach (Svenskt Vatten (SV) 2016), assuming constant rainfall intensity over 30 min for selected return periods, and a catchment area of 550 m^2. Design storms (1, 2, 5, 10, 20, and 50 years) were estimated using a national rainfall intensity equation (Dahlström 2010) (refer to Equation (2)). Target inflow rates were then calculated using the rational method.

$$i(T, t_r) = 190 \sqrt[3]{T} \frac{\ln (t_r)}{t_r^{0.98}} + 2 \tag{2}$$

where i denotes the rainfall intensity (L/(s ha)), T denotes the return period (months), and t_r is the rainfall duration (30 min for the studied cases). Mean inflow values ranged from 2.5 to 8.7 L/s, which corresponds to 1- and 50-year return periods, respectively.

2.2. Hydrological model

The storm water management model (SWMM) is well known for its ability to provide dynamic rainfall–runoff relationships for long-term simulations and to represent the main hydrological processes governing runoff generation (Rossman 2015). A SWMM model was set up to simulate runoff from a small catchment comprising a road section with an adjacent swale of the following physical characteristics: a hypothetical 0.055-ha (550 m^2) subcatchment, with 100% impervious cover, a gentle slope of 0.64%, a Manning roughness coefficient of 0.0013, and a depression storage of 1.5 mm typical for paved areas on flat slopes (refer to Table 2) (UDFCD 2016). These characteristics represent a road adjacent to the GS used as the study site (refer to Figure 1) (Mantilla *et al.* 2024). The system was modeled as a series of rectangular subcatchments as suggested by Gironás *et al.* (2009), where all runoff from the subcatchment was routed directly to the GS. Dynamic wave routing was used to solve the one-dimensional Saint-Venant equations and incorporate the continuity and momentum equations (Rossman 2015).

The GS was modeled as a separate subcatchment for better control of infiltration parameters based on the Green-Ampt method, such as the suction head (Ψ), saturated hydraulic conductivity (*ksat*), and the initial moisture deficit (IMD) (Green & Ampt 1911). The use of this procedure was necessitated by the lack of a configured set of swale infiltration parameters required for modeling the facility with the low impact development controls available in SWMM. The model represents each subcatchment as a non-linear reservoir and considers the main hydrologic processes occurring in the system (surface runoff, infiltration, and ET).

It is important to emphasize that the surface runoff runs perpendicularly to the width of the subcatchment, and the model only represents vertical infiltration along the swale bottom, neglecting the flow infiltrating on the side slopes, which serves as a stormwater quantity control mechanism (García-Serrana *et al.* 2017). The physical characteristics of the GS correspond to a section of 30 m with an average width of 5.2 m and a slope of 0.7%, which were earlier identified as the main physical parameters that govern surface runoff (Ekka *et al.* 2024) (refer to Table 2). A depression storage of 7 mm and a Manning roughness coefficient, $n = 0.2$, were used as typical values representing a vegetated surface (refer to Table 2) (Yen 2002).

Grassed swale simulations were driven by 15-min resolution climate data (precipitation, air temperature, ET, and wind speed) for each urban area (Luleå, Gothenburg, and Östersund). To assess the impact of different *ksat* values on overflow generation, simulations with swale infiltration rates of 2, 4, 11, 25, and 31 mm/h were carried out. The lowest rate (2 mm/h) was obtained from two iterations of a full-scale infiltration test conducted at the study site during the summer of 2022 and 2024 (Mantilla *et al.* 2024). Furthermore, point measurements using a Modified Philip–Dunne (MPD) infiltrometer were done and revealed high spatial variability in $ksat_t$, ranging from 13 mm/h at the swale bottom to 98 mm/h on the side slope. Ahmed *et al.* (2015) also reported large variability in infiltration rates, with geometric mean *ksat* values ranging from 7.5 to 390 mm/h – higher than

Table 2 | Summary of parameters of a hypothetical catchment used in SWMM

Parameter	Description	Value	Units
Subcatchment 1: Adjacent roadway[a]			
Area	Area of subcatchment	0.055	ha
Length	Length of the roadway	50	m
Slope	Average surface slope	0.64	%
% Imperviousness	Percent of impervious area	100	%
N-Impervious area[b]	Manning's n of impervious areas	0.013	unitless
% Zero-Imperviousness[b]	Percentage of impervious area with no depression storage	100	%
Dstore-imperv[b]	Depression storage in an impervious area	1.6	mm
% Routed	Percent runoff routed between sub-areas	100	%
Subcatchment 2: Grass swale			
Area[b]	Surface area of GS	0.0156	ha
Width[b]	Average width of GS	5.2	m
% Slope[b]	Average slope along the GS	0.7	%
N-pervious area[c]	Manning's n of pervious area	0.20	unitless
Dstore-perv[c]	Depression storage in the pervious area	7	mm
Infiltration parameters: Green-Ampt method			
Suction head[d]	Soil capillary suction along the wetting front	80	mm
Conductivity[e]	Soil saturated hydraulic conductivity	2, 4, 11, 25, and 31	mm/h
Initial deficit[e]	Fraction of soil volume that is initially dry	0.1	fraction

[a]Physical characteristics of the study site were taken from a topographical survey.
[b]Physical characteristics of an impermeable surface according to UDFCD (2016).
[c]Properties of a grass surface according to Yen (2002).
[d]Soil properties for a loamy sand soil texture according to Rawls *et al.* (1983).
[e]Infiltration rates and soil initial moisture content based on field experiments (Mantilla *et al.* 2024).

those applied in the present study. The results of point infiltration measurements at six GS subsections and three locations (right slope, left slope, and swale bottom) are presented in Supplementary Table S2a.

2.3. GS model calibration

The calibration of the swale model in SWMM focused on infiltration parameters according to the Green-Ampt method, including suction head (Ψ), *ksat*, and initial soil moisture deficit (refer to Table 3). An optimization approach was used to evaluate the goodness-of-fit between the observed and simulated peak outflow by estimating the mean squared error (MSE). The range of rainfall intensities was used as model inputs, covering low to high intensities represented by return periods between 1 and 50 years. These return periods correspond to irrigated inflows during field experiments (Mantilla *et al.* 2024). For each iteration of the optimization, the SWMM model input file was updated with the current parameter values (initial soil moisture deficit, *ksat*, and suction head) until the MSE converged to a minimum specified tolerance. This process was conducted individually for each return period, resulting in a set of calibrated parameters for return periods equivalent to 1, 2, 5, 10, 20, and 50 years. This suggests that the model requires higher infiltration rates (*ksat*) to manage severe rainfall events, compensating for higher runoff flows to match the observed outflow. The calibrated parameters for the suction head showed a narrow range of values, between 59 and 73 mm. The initial deficit remained constant at 0 across all return periods, aligning with field experiments, in which high initial soil water contents were maintained at the onset of irrigation.

The initial soil moisture deficit (IMD) parameter in SWMM was specified as 0.1, representing near-saturated antecedent soil conditions. This choice reflects the field irrigation experiments, in which the GS was deliberately pre-wetted to high soil moisture levels at the onset of testing, and introduced a condition such as a 'worst-case' scenario to evaluate the retention capacity of a GS (Mantilla *et al.* 2024). These conditions are consistent with observations from operational swales in northern Sweden, where shallow groundwater maintains high antecedent water contents (Rujner *et al.* 2018). To assess model sensitivity, IMD values were varied within a physically realistic range limited by soil porosity. For the loamy sand soil texture of the studied swale, porosity

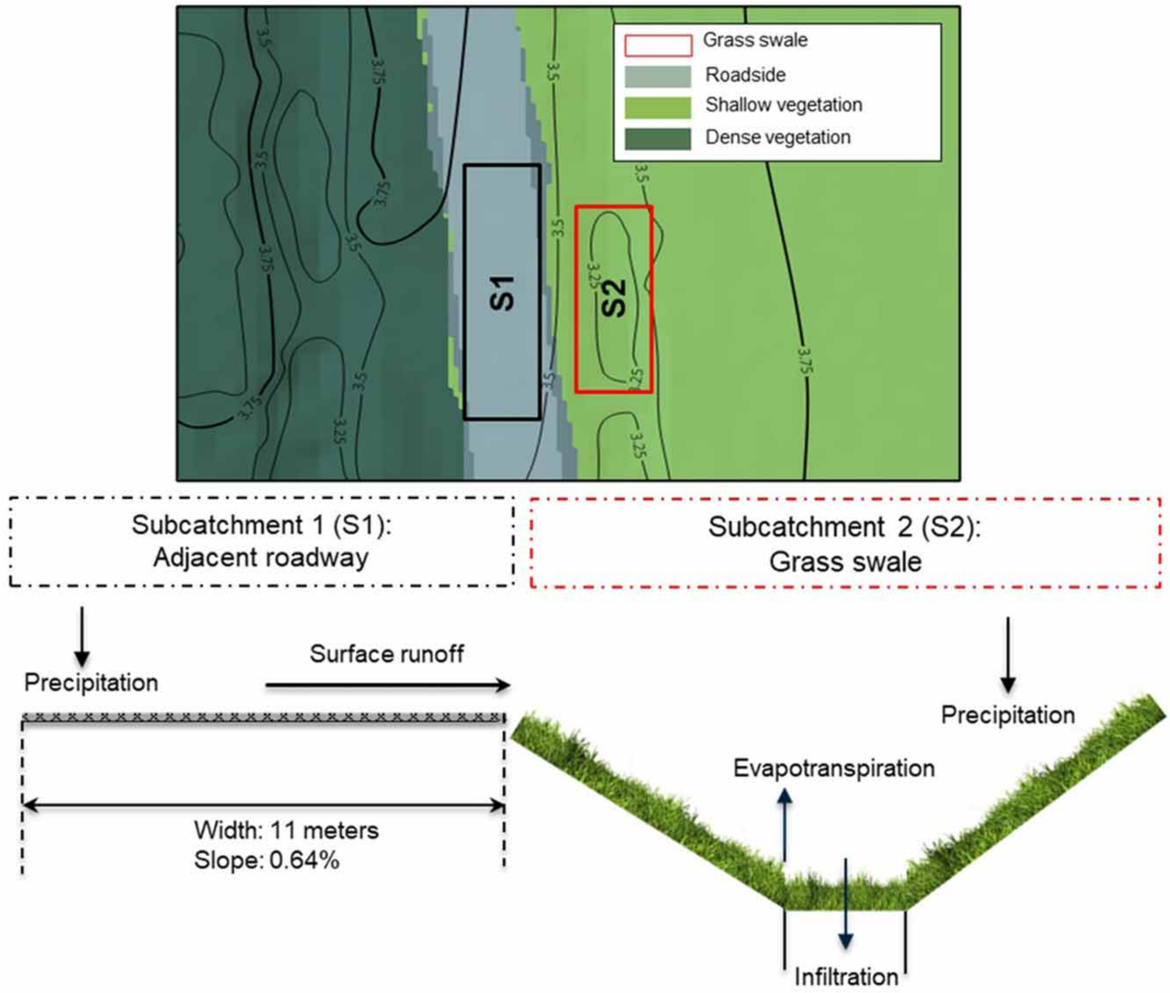

Figure 1 | Scheme of the modeled subcatchment in SWMM, with land-use categories of the catchment area.

Table 3 | Range of parameters used for calibrating the GS model in SWMM for different return periods

Parameter	Lower bound	Upper bound
ksat (mm/h)[a]	1	20
Initial deficit (%)[b]	0.0	0.45
Suction head (Ψ) (mm)[c]	50	150

[a]Initial deficit bands were chosen based on soil moisture content values (irrigation experiments).
[b]Range of *ksat* values measured with a Modified Philip–Dune infiltrometer.
[c]Suction bands represent values for loamy sand and sandy loam soil textures (Rawls *et al.* 1982).

values are typically between 0.35 and 0.45 (Rawls *et al.* 1982), and therefore, the tested IMD values did not exceed this upper bound (refer to Table 3). Values beyond soil porosity were excluded, as these would be physically unrealistic and would not represent plausible storage conditions in the soil profile.

After calibration for each return period, the mean value of each calibrated parameter was estimated across all scenarios (refer to Table 4). This provides a single parameter set that balances performance across different conditions. In terms of the calibration performance, NSE values were slightly negative for the smallest return periods (–0.15 for 2 years) but became positive for the periods of 5 years and larger, with the highest value of 0.42 for the 50-year event. KGE ranges from 0.27 (2 year) up to 0.67 (50 year), with a mean of 0.44 – considered a 'satisfactory' fit of the observed outflow rates. The calibrated parameters showed higher ksat values for greater return periods (refer to Table 5).

Table 4 | Calibrated parameters of the GS model in SWMM for different return periods

Parameter	Return periods 1	2	5	10	20	50	Mean
Inflow rate (L/s)[a]	2.5	3.1	4.2	5.2	6.4	8.7	
ksat (mm/h)[b]	8.7	17.7	37.6	66.5	100.8	132.5	61
Initial deficit (%)[c]	0.1						0.1
Suction head (Ψ) (mm)[d]	59.8	58.9	59.1	64.8	62.0	72.5	2.44
NSE[e]	−0.03	−0.15	0.09	0.17	0.08	0.42	0.10
KGE[e]	0.36	0.27	0.43	0.46	0.42	0.67	0.44

[a]Inflow rates (L/s) represent different return periods, from 1 to 50 years.
[b]Initial deficit bands were chosen based on soil moisture content values (irrigation experiments).
[c]Range of *ksat* values measured with a Modified Philip–Dune infiltrometer.
[d]Suction bands represent values for loamy sand and sandy loam soil textures (Rawls *et al.* 1982).
[e]NSE and KGE values represent Nash–Sutcliffe efficiency and Kling–Gupta efficiency values.

Table 5 | Mean characteristics of GS overflow risk under different *ksat* values

Urban area	*ksat*	Mean annual overflow events[a]	Mean annual overflow volume (m^3)[b]	Mean annual risk (m^3/year)[c]
Göteborg	2	60	185.0	236.2
	4	43	115.6	107.0
	11	17	36.1	13.7
	25	6	10.6	1.6
	31	4	7.7	0.8
Luleå	2	26	82.9	64.3
	4	17	52.6	27.4
	11	7	18.4	4.1
	25	3	6.1	0.7
	31	2	4.5	0.4
Östersund	2	26	81.7	10.4
	4	17	52.1	4.5
	11	7	18.4	0.7
	25	3	6.1	0.1
	31	2	4.5	0.0

[a]Mean annual overflow events were estimated during the entire period of simulation (1997–2019), aggregated on an annual basis.
[b]Mean annual overflow volume is estimated as the sum of volume aggregated on an annual basis.
[c]Annual overflow risk was estimated as the product of the annual probability of overflow (from 0 to 1) and the annual overflow volume (m^3).

2.4. Risk determination and acceptable operation

This assessment focuses on the contribution of the physical design parameters of a GS (*ksat*) to reducing flood risk, following an approach adopted by Lewellyn & Wadzuk (2019). The risk assessment employed referred to the combination of the probability, or frequency of a defined hazard, and the magnitude of its consequences (Skivington 1997). In the present study, the first component of the assessment represents the probability (P_{over}) of occurrence of an overflow event. The second component is referred to as the consequence, corresponding to the overflow volume or untreated volume ($C_{over,v}$) (refer to Equation (1)). Therefore, in the present study, GS overflow risk is defined as the expected annual volume of unmanaged runoff from the swale, computed as the product of the probability of an overflow event and its overflow volume.

$$\text{Risk}\,(\text{m}^3/\text{year}) = P_{\text{over},v} * C_{\text{over},v} \tag{3}$$

The analysis was conducted on an annual basis for months with precipitation in the form of rainfall (excluding snowfall), using historical time series spanning the simulation period from 1997 to 2019. The probability of overflow was estimated by identifying the number of overflows per year and dividing it by the number of annual days. This term represents a probability ranging from 0 to 1. The consequence corresponds to the volume of overflow expressed in m^3 ($V_{total,v}$), which occurs when the storage capacity (surface and soil storage) is exceeded, resulting in unmanaged (uncontrolled) runoff from the drainage area. The estimation of total risk of overflow is expressed as m^3/year, which results from the product of the annual probability of overflow and the cumulative annual volume of overflow. Similarly, this study defines acceptable operation as the system's ability to meet a stormwater control target, ensuring no overflow that would create adverse downstream impacts. The threshold is set at 10 cm water depth (below the 12 cm grass height), corresponding to an overflow volume of 15.6 m^3 based on a 156 m^2 surface area. Exceedance curves for different *ksat* values in Gothenburg, Luleå, and Östersund illustrate the percentage of the wet period when the facility operates below this threshold. This analysis helps determine the minimum *ksat* needed to reduce overflows and minimize failure mode operation.

The threshold for acceptable GS operation was defined as a maximum ponding depth of 10 cm, which is below the 12 cm grass height and prevents persistent standing water. To translate this depth into a volumetric threshold, the swale surface area (156 m^2; length 30 m $\times$ mean width 5.2 m) was multiplied by the ponding depth (refer to Equation (4)).

$$V = A \times h = 156\,\mathrm{m}^2 \times 0.10\,\mathrm{m} = 15.6\,\mathrm{m}^3 \tag{4}$$

This threshold volume was then used as a benchmark against SWMM output parameters. Specifically, the *surface runoff outflow* (m^3) from the swale subcatchment was extracted, and cumulative exceedance was compared against the 15.6 m^3 threshold to determine when the system entered failure mode.

A series of exceedance curves is presented for each urban area and infiltration rate. Annual runoff depths are converted to swale overflow volumes (m^3) and plotted against the percentage of time the swale infiltration capacity is exceeded. A horizontal line at 15.6 m^3 marks the design threshold, with green shading below (acceptable) and red above (overflow) (see Figure 2). The objective is to show, for each *ksat*, how higher infiltration rates reduce both overflow volumes and the frequency of threshold-exceeding events, thereby identifying the minimum *ksat* required for resilient swale design. In addition, an event-based analysis was conducted, showing individual rain events that exceeded the swale infiltration capacity, focusing on those overflow volumes that surpassed the 100 mm equivalent threshold. Histograms of event overflow volumes (m^3) illustrate how rainfall characteristics (intensity and total volume) in each urban area drive overflow occurrence (see Figure 2).

3. RESULTS

3.1. Annual number of overflows and their volume

The number of overflows varied among the years for each urban area, and corresponded to changes in local climatic conditions, including the total annual precipitation. As expected, the number of annual swale overflows declined with increasing *ksat* values. For Gothenburg, the highest number of overflow events, $N = 85$, was observed for an assumed *ksat* of 2 mm/h (note that the literature recommends the minimum or applicable swale hydraulic conductivity of 12 mm/h; US EPA 2021). A reduction of 93% in swale overflows was achieved at a *ksat* of 31 mm/h, resulting in a mean of four overflow events per year (refer to Figure 3). Greater annual variability in swale overflows was observed at lower *ksat* values (2 and 4 mm/h), with standard deviations (SD) of 15 and 11 annual events, respectively (refer to whiskers in Figure 3(a)). Swale overflows led to mean annual volumes ranging between 185 and 8 m^3 (for a *ksat* of 2 and 31 mm/h, respectively) (refer to Figure 3(d)). The maximum overflow volume occurred in a year with a total rainfall of 722 mm, which did not represent the year with the highest number of overflow events. This finding indicates that the number of overflow events is influenced not only by the total annual rainfall volume but also by the intensity of rainfall events, specifically the frequency of events with an intensity that exceeds the capacity of the swale to retain runoff.

In contrast, Luleå exhibited the lowest number of GS overflows among the three urban areas, with a mean overflow of 26 events for a *ksat* value of 2 mm/h and 2 events for a *ksat* value of 31 mm/h. The largest number of overflows occurred in the year with a total annual rainfall of 536 mm (refer to Supplementary Table S2b), which represents the second-highest annual rainfall during the analysis period. This annual rainfall resulted in an overflow volume of 120 m^3. Conversely, no overflow events were observed for *ksat* values of 25 and 31 mm/h, in the year with an annual rainfall of 202 mm. Overall, the mean annual overflow volume ranged between 83 and 5 m^3 for *ksat* values of 2 and 31 mm/h, respectively. It is important to note that Luleå experiences snowfall for approximately 5 months of the year, with higher rainfall typically occurring in July and

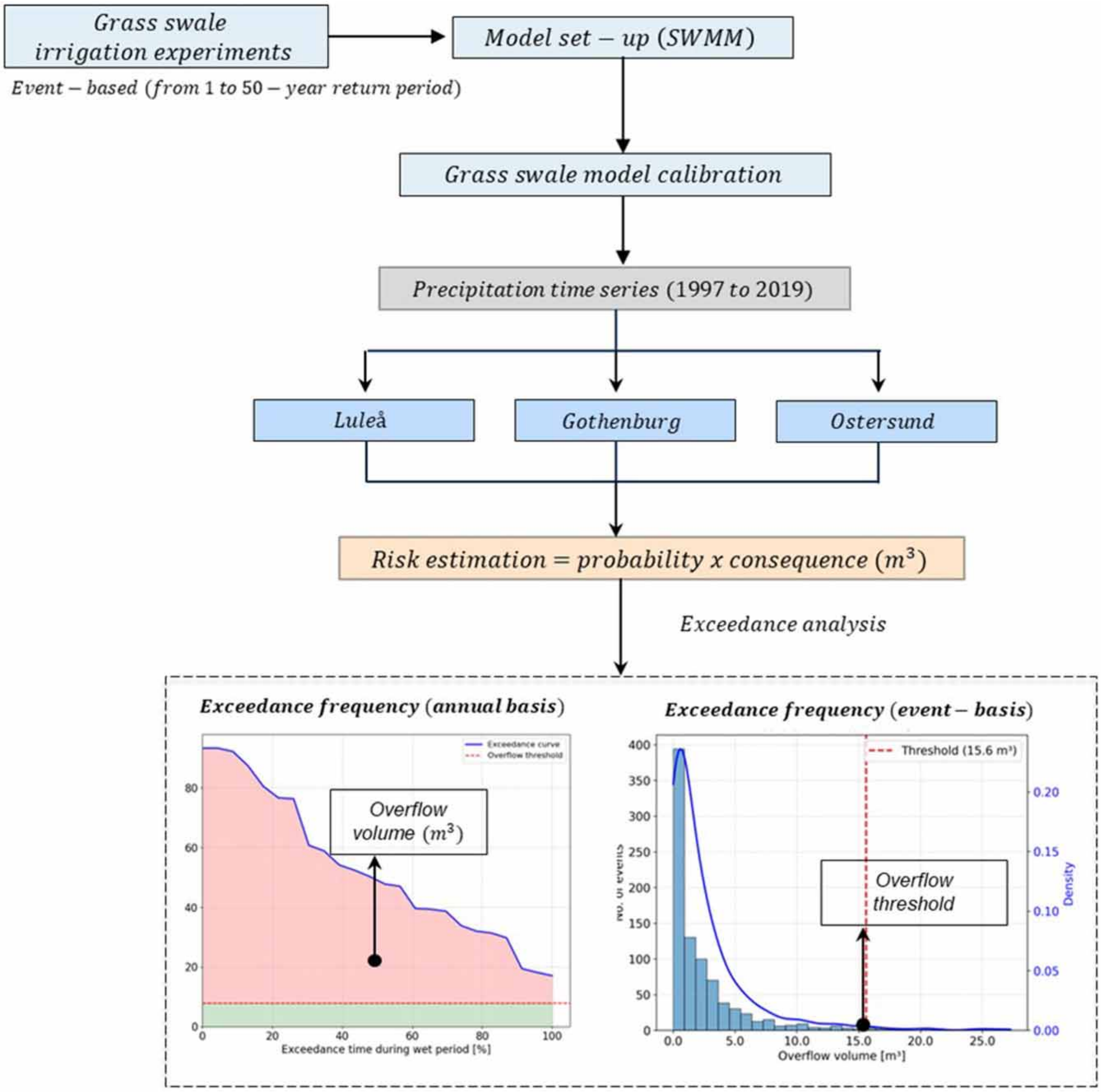

Figure 2 | Schematic of the swale risk-based methodology.

August. This narrow precipitation window resulted in lower variability in overflow occurrences (refer to Figure 3), with SDs of seven and five events for *ksat* values of 2 and 4 mm/h, respectively.

Results in Östersund were consistent with those from other areas, showing a declining trend in overflow occurrences with increasing *ksat* values. The annual number of overflows ranged from a mean of 30 occurrences at a *ksat* of 2 mm/h to 2 occurrences at a *ksat* of 31 mm/h, and resulted in mean annual volumes ranging between 82 and 5 m^3, respectively. No overflows were observed at the highest *ksat* values of 25 and 31 mm/h in 2002, the year with a total annual rainfall of 302 mm (below the mean annual rainfall for the period of analysis). Similar overflow occurrences were observed at higher *ksat* values (25 and 31 mm/h), with mean occurrences of 3 and 2, respectively (refer to Supplementary Table S2c).

Swale overflow analysis using the recommended *ksat* of 11 mm/h showed overflow reductions of 71% in Gothenburg, 10% in Luleå, and 8% in Östersund, compared with 2 mm/h. However, *ksat* >12 mm/h was insufficient to fully capture rainfall events at any location. A minimum *ksat* of 25 mm/h limited overflows to $\leq$6 events per year, with a mean maximum annual overflow volume of 10.6 m^3 in Gothenburg – below the acceptable threshold of 15.6 m^3 (equivalent to 10 cm water depth). Further analysis is needed to ensure that downstream systems can handle this volume without adverse impacts, including the gradual release of flow at a rate of $\leq$2 L/s ha, as recommended by Ballard *et al.* (2015).

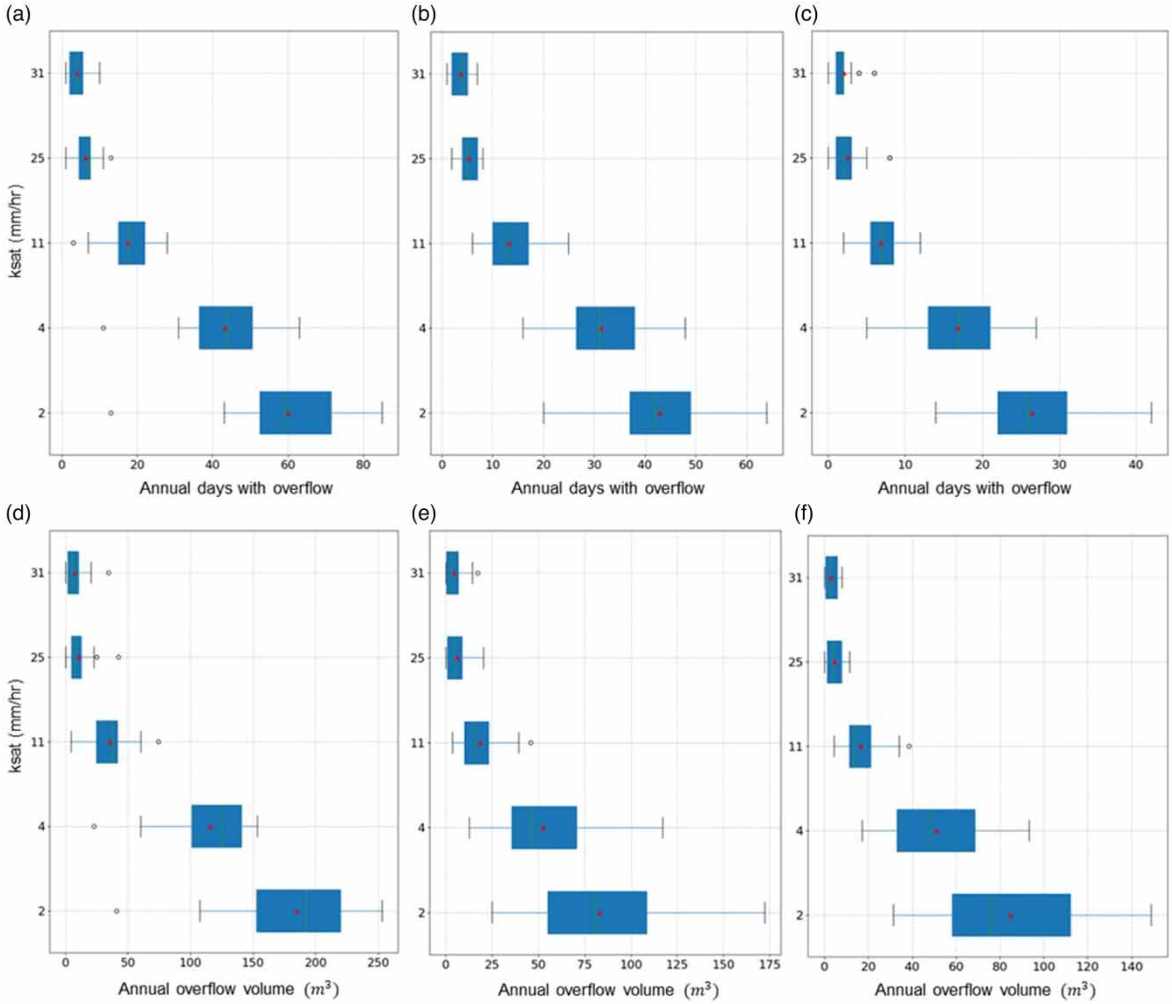

Figure 3 | Number of days with overflow occurrences and overflow volume per year, for different *ksat* values. (a and d) Refer to Gothenburg, (b and e) to Luleå, and (c and f) to Östersund.

A Tukey HSD test was conducted to assess overflow risk differences across *ksat* values. In Gothenburg, increasing *ksat* from 2 to 11 mm/h significantly reduced overflow volumes ($\Delta = 42.5$ m^3, $p < 0.001$), but further increases beyond 25 mm/h had negligible effects ($\Delta = -2.2$ m^3, $p = 0.926$) (Supplementary Table S3a). In Luleå, the largest overflow reduction occurred between 2 and 25 mm/h ($\Delta = 48.2$ m^3, $p < 0.001$), with a further increase to 31 mm/h resulting in a significant overflow decrease ($\Delta = -48.3$ m^3, $p < 0.001$) (Supplementary Table S3b). Similarly, in Östersund, the greatest reduction was observed between 2 and 25 mm/h ($\Delta = 60.4$ m^3, $p < 0.001$), with additional decreases beyond 25 mm/h (Supplementary Table S3c). These results suggest that 25 mm/h is a critical threshold, beyond which overflow reductions vary by location.

An analysis of the correlation between the annual risk of overflow (m^3/year) and mean annual rainfall (mm) showed a strong positive trend for Gothenburg and Lulea for *ksat* values of 2 and 4 mm/h ($r^2 > 0.7$) (refer to Figure 4(a) and 4(b)). In contrast, the annual risk of overflow in Östersund showed lower correlation coefficients for all *ksat* values, with the highest correlation ($r^2 > 0.5$) for a *ksat* of 2 mm/h (refer to Figure 5(c)). While overflow risks were found to strongly correlate with total annual rainfall for Gothenburg and Luleå, in Östersund, additional factors drive the occurrence of overflows for low *ksat* values. These factors include the presence of higher ET rates that help restore soil retention capacities during dry periods, thereby reducing soil moisture contents at the onset of rainfall events. Rujner *et al.* (2018) found that higher initial soil moisture contents led to a reduction of the available pore space in the soil media, which limited the retention capacity of a GS.

Regardless of the magnitude of *ksat*, it was observed that overflow risk was below 11 and 15 m^3 for annual rainfall <400 mm in both Luleå and Östersund, respectively (refer to Figure 4(b) and 4(c)). In the case of Gothenburg,

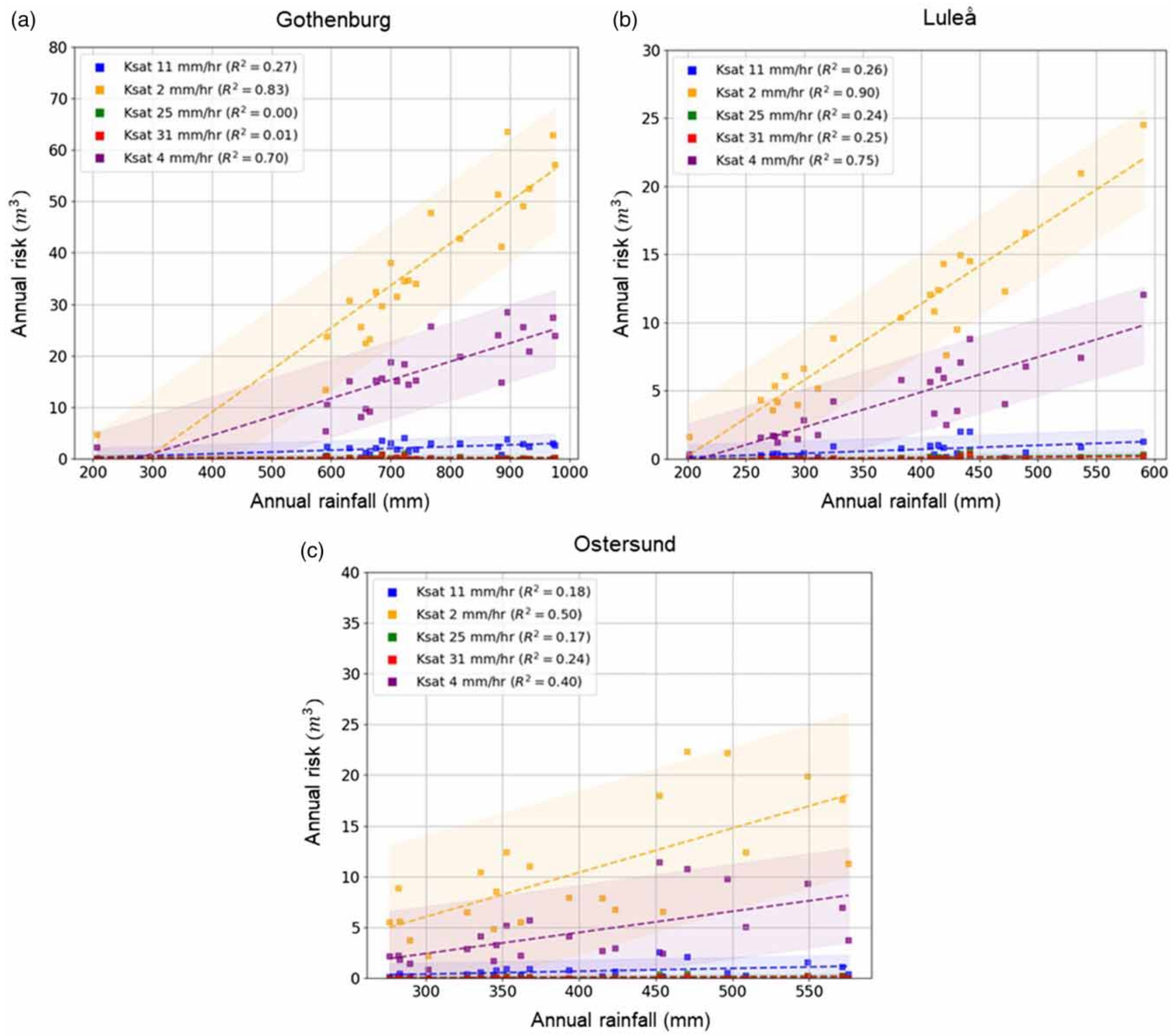

Figure 4 | Annual overflow risk (m^3/year) with respect to annual rainfall (mm) for different *ksat* values. Dots represent annual values across the simulation period. The shaded band represents 95% confidence intervals.

the higher annual risk was observed for an annual rainfall of 895 mm, leading to the highest annual risk of 63 m^3 (refer to Figure 4(a), under a *ksat* of 2 mm/h). For low infiltration capacities, the hydrological response is dominated by surface runoff rather than infiltration, evaporation, or initial abstraction, making the flood risk a direct function of total precipitation (Lhamidi *et al.* 2024). Lewellyn & Wadzuk (2019) found that regardless of the *ksat* of biofilter cells, there is a very low risk of overflow for rainfall events less than approximately 5 mm in depth. However, it is important to highlight that the design structure of biofilter cells allows such facilities to store water on their surface, which could provide an additional storage volume before the overflow occurs. Conversely, the same authors found that for moderate infiltration rates of 12.7 mm/h, there were no overflow occurrences for rainfall events with depths less than 15 mm.

3.2. Overflow exceedance on an event basis

An event-based analysis was conducted to estimate how many individual events exceed an overflow threshold of 15.6 m^3 for each urban area under different *ksat* values. The number of overflow events was driven by the local climatic conditions and the swale infiltration capacity. Across all six plots (see Figure 5), the event-volume distributions are strongly right-skewed, with most overflow events producing small volumes (often under 2 m^3), and a long tail of progressively larger overflows. The majority of events fall into the smallest bin, indicating that most of the events barely exceed the swale's capacity. Under low infiltration (*ksat* = 2 mm/h, left column in Figure 5), Gothenburg shows the highest number of exceedances, while Östersund exhibits the lowest (14 events). Under

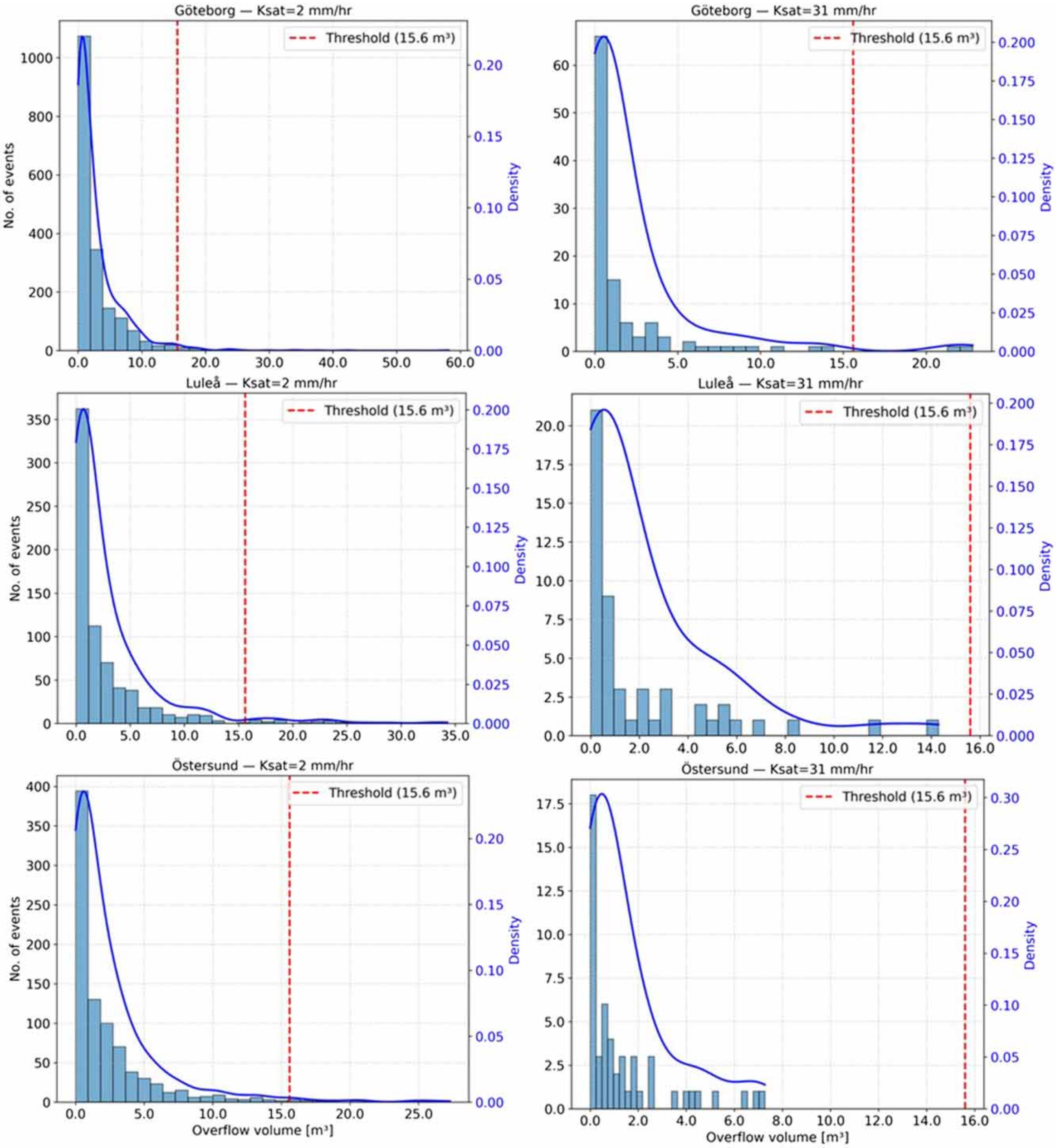

Figure 5 | Overflow event-volume histograms (primary *y*-axis) and density curves (secondary *y*-axis) for Göteborg, Luleå, and Östersund at *ksat* = 2 mm/h (left) and 31 mm/h (right). The red dashed line shows the 100 mm depth threshold (15.6 m^3).

high infiltration (*ksat* = 31 mm/h, right column), overflow volumes drop markedly, with only two events in Gothenburg and no overflows in Luleå or Östersund (refer to Figure 5).

Across all three sites, increasing the infiltration parameter (*ksat*) reduces both the total number of runoff events and the frequency of overflows (those exceeding 100 mm depth, or 15.6 m^3), with different reductions depending on the type of climate. In Gothenburg, raising *ksat* from 2 to 31 mm/h decreases overflow occurrences by 95%, while the mean overflow volume of the remaining exceedance events holds steady at about 23–26 m. In Luleå, no threshold exceedances occur once *ksat* reaches 25 mm/h, meaning that high infiltration completely prevents swale overflow in a cooler, less-intense climate. These conditions indicate that when exceedances occur at lower *ksat*, their mean volumes (≈18–22 m^3) are smaller than in Gothenburg, reflecting fewer large rain events. Östersund exhibits a similar pattern to Luleå but with even fewer exceedances: at *ksat* = 2 and 4 mm/h, there are 20 overflow events (and a mean overflow volume around 20), but none once *ksat* ≥11 mm/h.

To evaluate the effect of IMD on the overflow occurrence, Figure 6 shows that as the swale initial soil deficit increases from 0.1 to 0.8 (i.e., from nearly saturated toward dry conditions), the total number of runoff events decreases – from 120 to 63 – demonstrating that drier antecedent conditions absorb more small-to-medium rainfall events without producing any runoff. Meanwhile, the mean volume of those few storms that still generate overflow declines (from about 22.1 m^3 at low deficit to 21.0 m^3 at high deficit). Rujner *et al.* (2018) found similar results in a 30-m swale section, showing that under low soil moisture content, the facility reduced runoff by up to 82%, whereas high moisture content yielded runoff reductions as low as 15%.

3.3. Acceptable GS operation

Exceedance curves are presented to evaluate the percentage of time the GS operates in failure conditions under different *ksat* values. In general, the slope of the exceedance curve becomes steeper with increasing *ksat* values (for all three urban areas), indicating an increase in the proportion of time the system operates within the acceptable range. Findings showed annual variability in overflow occurrences under the same *ksat*, thereby leading to differences in acceptable operation across the simulation period. Results show that having a *ksat* of only 2 and 4 mm/h will lead to facilities operating in a failure mode 100% of the time (refer to Figure 7 for the three locations).

For Gothenburg, at low *ksat* values (2 and 4 mm/h), the overflow volumes are significantly higher, exceeding 250 and 160 m^3, respectively. These results indicate that 100% of the wet period experiences overflow volumes above an acceptable threshold of 15.3 m^3. A minimum *ksat* of 25 mm/h is necessary to achieve acceptable operation for more than 50% of the time, which is not sufficient to completely avoid overflow events. Furthermore, with a *ksat* of 31 mm/h, the overflow volumes are further reduced, with mean annual overflow volumes of 7.7 m^3, leading to acceptable performance for around 70% of the time.

A similar trend was observed in Luleå, with the GS operating in failure mode (above the acceptable threshold) 100% of the time under *ksat* values of 2 and 4 mm/h (refer to Figure 7(d)). A reduction in the mean overflow volume from 175 to 40 m^3 was achieved when increasing the *ksat* to 11 mm/h, compared with the minimum infiltration rate of 2 mm/h (refer to Figure 7(b) and 7(e)). While a significant reduction in maximum overflow volume was achieved with the highest *ksat* of 31 mm/h, leading to volumes below 18 m^3, the swale still operates in failure mode for approximately 20% of the time. Overall, compared with Gothenburg, lower *ksat* values are required to achieve a greater proportion of time with acceptable operation. These findings are attributed mainly to lower annual rainfall volumes in Luleå, with a shorter rainfall period (between June and October).

Results in Östersund showed longer periods of acceptable operation with *ksat* values of 11, 25, and 31 mm/h, when compared with Gothenburg and Luleå. A reduction in annual overflow volume below 10 m^3 was observed under a *ksat* of 31 mm/h, leading to acceptable operation 100% of the time. These results indicate that Östersund was the only urban area without operating in failure mode under the highest *ksat* value. The exceedance curves suggest that precipitation patterns in Östersund are more favorable for GS implementation for runoff control compared with Gothenburg and Luleå. This is due to moderate annual precipitation evenly distributed

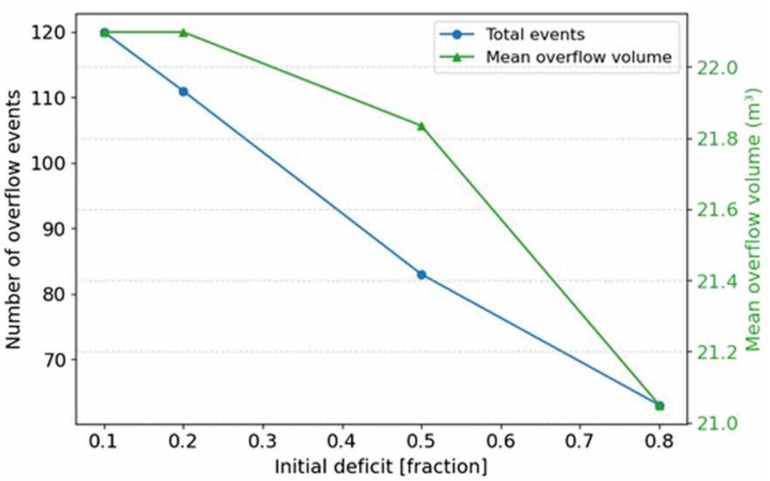

Figure 6 | Overflow count (primary axis) and mean overflow volume (secondary axis) vs. initial soil deficit for *ksat* = 31 mm/h.

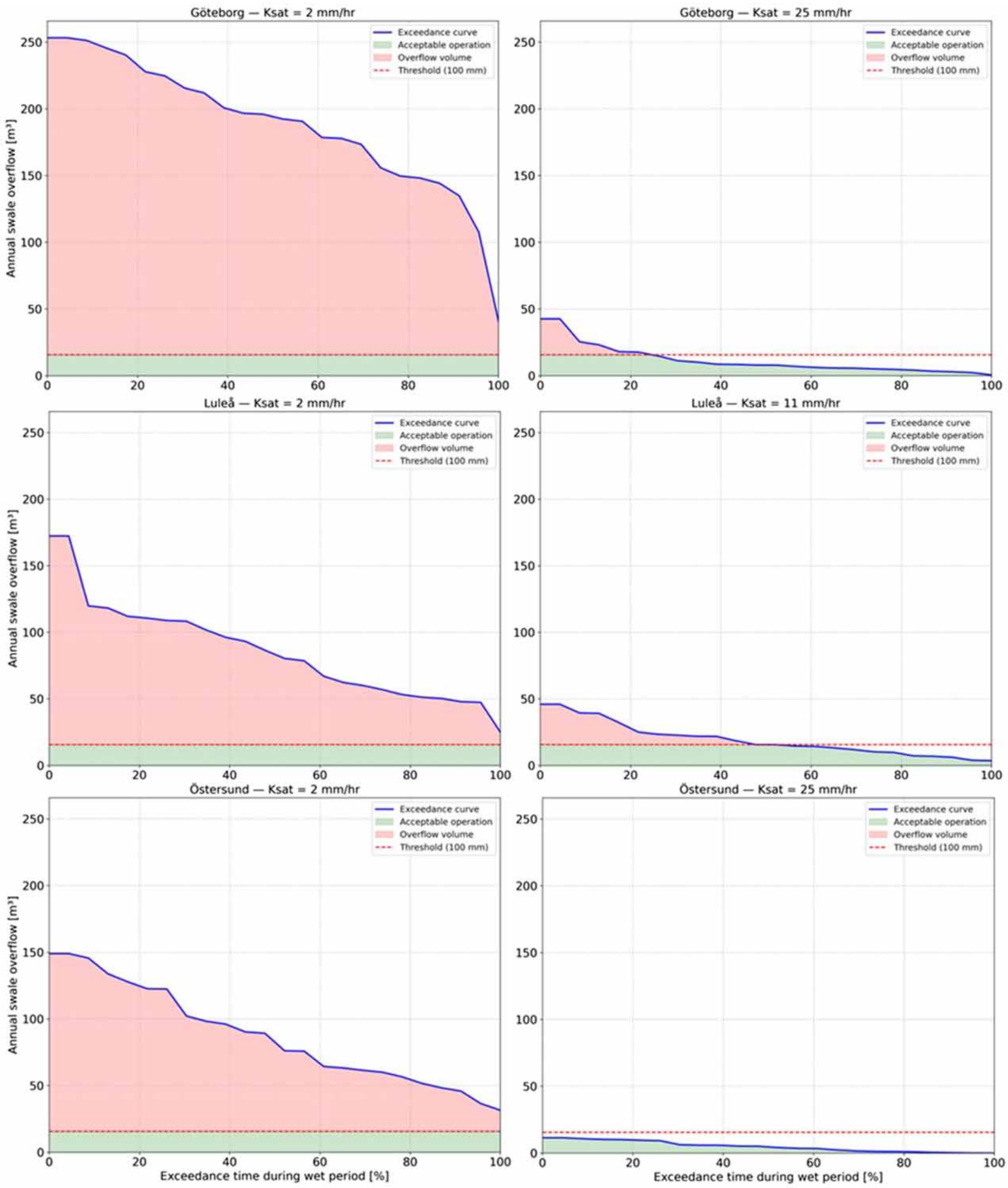

Figure 7 | Exceedance curves showing the percent of wet-weather time with an acceptable operation of the GS under different *ksat* values. The dashed red line corresponds to an overflow threshold (15.6 m^3). The shadow green area corresponds to an acceptable operation.

throughout the year, with the absence of high-intensity rainfall events, characteristic of both maritime and oceanic climates (Köppen & Geiger 1936). Results also showed that with a *ksat* of 31 mm/h, there is potential for greater retention volumes, suggesting that a larger contributing catchment area could be connected to the swale.

4. DISCUSSION

4.1. Implications of a risk-based assessment for swale design

The adoption of a risk-based design approach has been widely considered in fields such as flood management of river deltas (De Bruijn *et al.* 2014), sewer rehabilitation (Korving *et al.* 2009), catastrophe management (Park *et al.* 2013), or assessment of environmental contamination (e.g., organic micropollutants) in freshwaters from biofilter cell discharges (Beryani *et al.* 2023). However, this approach is not traditionally implemented in evaluating the design of GSI for reducing flood risk (Lewellyn & Wadzuk 2019). The methodology adopted in the present study shows how the overflow risk in grass swales is influenced by three main factors: (1) local climate conditions (including annual rainfall and interevent conditions), (2) soil permeability (e.g., saturated hydraulic conductivity and erodibility), and (3) swale design parameters (e.g., cross-section dimensions, longitudinal slope, and channel roughness).

Overall, the results presented as exceedance curves provide an indication of the different rainfall patterns at the three locations and the necessary design characteristics to achieve acceptable performance. For instance, Gothenburg experiences frequent rainfall throughout the year, without marked dry periods, and higher rainfall intensities, characteristic of an oceanic climate (Köppen & Geiger 1936), leading to a higher likelihood of overflow occurrences. Results presented suggest that at locations with rainfall patterns similar to Gothenburg, where native soils (e.g., predominant with silt loam or clay) do not achieve the minimum recommended infiltration rate of 12 mm/h (US EPA 2021), additional design considerations should be taken into account. These include a greater cross-sectional area to maximize the conveyance capacity, such as increasing the swale width (Ekka *et al.* 2024), or inserting an underdrain below the swale bottom. When space is limited, Winston *et al.* (2017) suggested using a longer section of a triangular channel with side slopes 6:1 (H:V). Ahmed *et al.* (2015) found that avoiding compaction in the main channel during the construction phase of grass swales is crucial to maintain soil permeability. Furthermore, an additional surface storage capacity could be achieved by introducing outflow controls, providing extra retention volume in existing facilities (Mantilla *et al.* 2024).

Rodriguez *et al.* (2021) used a similar approach to evaluate the resilience of three types of GSI – a biofilter cell, a section of permeable pavement, and a green roof – by analyzing system failure using stress–strain curves. Similarly, Rodriguez *et al.* (2023) used a global resilience analysis to evaluate the capacity of GSI to reduce combined sewer overflows by characterizing rainfall patterns (such as the magnitude and frequency of heavy rainfall events). This approach allowed the identification of conditions under which GSI fails to maintain an acceptable level of service – evidenced by severe sewer surcharging, flooding, and combined overflows that harm water quality and summer recreation. Similarly, Winston *et al.* (2016) used exceedance curves to evaluate whether three biofilter cells with low hydraulic conductivity could eliminate outflows from small events, showing that the minimum rainfall depths required to produce outflows were 5.5, 7.4, and 13.8 mm for the three biofilters studied. The same study found that increasing ponding depths by up to 51% (corresponding to an additional 5–17 cm) was necessary to reduce the occurrence of overflows under such rainfall depths (<13.8 mm). In terms of reducing flood damages by adopting GSI, Staccione *et al.* (2024) found that increasing GSI implementation by 25% (in terms of area required) in the City of Milan, Italy, could potentially halve the pluvial flood damages and reduce the population exposed to flood conditions by 40%.

While the present study evaluates the overflow risk based on historical rainfall, changes in rainfall conditions given by a non-stationary climate require adjustments to meet the future desired levels of service (Hathaway *et al.* 2024). Hathaway *et al.* (2014) determined that storage depths would need to be increased by 9–31 cm (while maintaining other design parameters constant) to restrict annual overflow from bioretention cells under future climate conditions in North Carolina, USA. Lewellyn & Wadzuk (2019) evaluated the overflow risk of a biofilter cell under different climate change scenarios, resulting in risk increments above the acceptable level for designs with a *ksat* of 25.4 mm/h and a ponding depth of 76 mm. The same study found that it would be necessary to work with soil media with a *ksat* of at least 51 mm/h to achieve a risk below the acceptable level. However, such infiltration rates (51 mm/h) can be found only in engineered soil media (in the case of biofilter cells), but are rarely found or sustained in native soils of grass swales (Mantilla *et al.* 2025). Hamouz *et al.* (2020) found that adding an expanded-clay layer beneath green-roof substrates improved detention during extreme precipitation due to climate change. Similarly, Pons *et al.* (2022a, b) forecasted green-roof performance at six sites (four in Norway, two in France), finding reduced detention in most Norwegian cities – especially Bergen – due to increased rainfall, and slight improvements in Marseille where event frequency decreased.

Despite the widespread use of GSI for reducing the adverse effects of urbanization and climate change, GSI performance can deteriorate over its lifecycle, leading to operational failures (Bahrami *et al.* 2024). To anticipate malfunctions and enhance the long-term performance of such facilities, the identification of conditions that lead to failure mode operations needs to be documented (Langeveld *et al.* 2022). This information can be used to recognize component vulnerabilities, required design modifications, and predictive strategies to maintain service levels (Cherqui *et al.* 2019). For instance, limited research has been conducted on the decline of performance of GSI over time, particularly with respect to accurately predicting changes in soil hydraulic properties, which directly affect stormwater retention capacities (Gonzalez-Merchana *et al.* 2012). Ensuring long-term performance in agreement with the initial GSI design, suitable monitoring and evaluation of soil properties changes in time, at different temporal scales, need to be undertaken (Le Coustumer *et al.* 2009). To account for seasonal variabilities, Paus *et al.* (2016) found that bioretention media with a sufficiently high *ksat* value (i.e., >10 cm/h) should be selected when designing such facilities for optimal hydrologic performance in cold climate regions.

It should be acknowledged that the 15.6 m^3 threshold, derived from a uniform 10 cm ponding depth across the swale footprint, represents an instantaneous exceedance criterion. However, this simplification does not capture all possible rainfall dynamics. For instance, a long-duration, low-intensity storm could generate cumulative overflow volumes greater than 15.6 m^3 without ever producing a 10 cm ponding depth at a single point in time. Similarly, numerous small rainfall events, each generating minor runoff volumes below the threshold, could cumulatively surpass the 15.6 m^3 annual total. These scenarios highlight that the threshold volume should be interpreted as a design benchmark for individual event exceedances rather than an absolute predictor of cumulative risk. To account for such conditions, our analysis combined threshold-based exceedance curves with annual risk estimates, which together capture both instantaneous depth exceedances and the cumulative contributions of frequent smaller events. This dual perspective provides a more robust assessment of swale performance under diverse rainfall regimes. Future work should further refine this approach by explicitly distinguishing between instantaneous ponding depth exceedances and cumulative annual overflow volumes, potentially through the use of coupled 1D–2D hydrodynamic models.

A key contribution of this study lies in the application of a risk-based framework, which extends beyond conventional event-based exceedance analyses. While event-based metrics provide information on the frequency and magnitude of individual overflow events, they do not capture how these events translate into long-term operational risk. The yearly risk-based approach integrates both the probability of occurrence and the cumulative consequences (overflow volumes), thereby offering a measure of expected annual risk that is more directly aligned with decision-making in design and management contexts. This provides two added benefits: (1) it allows for comparisons across sites and design scenarios on a common annualized scale and (2) it supports the integration of hydrological performance with broader flood risk management objectives, where risk is commonly defined as the product of likelihood and consequence. The findings presented here confirm earlier applications of risk-based methods in stormwater and sewer system design (e.g., Korving *et al.* 2009; Lewellyn & Wadzuk 2019), while demonstrating their utility in the specific context of GS performance. By linking exceedance analyses with a formal risk framework, our study translates hydrologic model outputs into a format that is directly usable for defining acceptable service levels and prioritizing adaptation strategies.

4.2. Limitations of the study

It is important to emphasize that the overflow results are governed by the physical characteristics of the GS being studied, such as the cross-sectional area and swale length. Due to limitations of the model used (a lumped, one-dimensional model) to represent important features of the GS – such as infiltration on the side slopes and variations in soil hydraulic conductivities, which have been found to influence the swale retention capacity (Mantilla *et al.* 2024) – the findings reported here might underestimate the swale capacity to retain runoff volumes. For instance, Apel *et al.* (2009) assessed the model complexity needed for flood risk assessments in a municipality in southeastern Germany and found that coupling 1D/2D hydraulic modeling with a multifactor flood-loss model best balanced data requirements, simulation effort, and result accuracy. The results presented do not aim to estimate the consequences of overflows in downstream urban areas (which would require a two-dimensional model), but rather to provide an overview of the influences of rainfall patterns, soil permeability, and physical swale properties on the acceptable performance of grass swales for stormwater retention. The estimated overflow risk is the result of the combination of the likelihood of overflow occurrence and the associated volume, but it does not indicate the acceptable level of risk, which would require balancing tolerable conditions for stakeholders with economic, social, environmental, and technical factors (Mens *et al.* 2011).

In addition, the GS was modeled as a separate subcatchment using the Green-Ampt infiltration method. This approach presents a limitation, given that the model does not dynamically restore soil moisture by actual evapotranspiration (PET) between rainfall events but instead uses a user-specified 'initial deficit' and assumes a constant recovery rate driven solely by the *ksat* (Rossman 2016). In practice, this means that antecedent moisture conditions in the swale media remain fixed or recover at a rate following each rainfall event, regardless of air temperature, solar radiation, or wind speed. As a result, simulations may overestimate infiltration (and thus underestimate overflow) when true soil moisture recovery is slower than *ksat* would imply – such as during cool, low-PET periods – or conversely underestimate infiltration after dry spells when actual PET would have further depleted soil moisture.

The values used for the model calibration (parameter bounds) were consistent with field evidence and soils literature (Table 3), yet the overall statistical performance remained modest across return periods (Table 4). NSE values were near zero or slightly negative for the smallest events (e.g., –0.15 for the 2 years) and improved with increasing inflow magnitude, reaching 0.42 for the 50-year event; KGE followed a similar pattern (0.27 → 0.67), with an overall mean of 0.44, which can be considered a satisfactory fit. This scale dependence likely reflects (1) a lower signal-to-noise ratio at small flows (measurement uncertainty and minor timing mismatches can penalize NSE/KGE disproportionately), (2) stronger control of antecedent moisture and lateral/frontal inflow partitioning during low-intensity tests, and (3) structural simplifications from representing the swale as a single subcatchment (which limits the description of heterogeneity and preferential flow). Event-wise calibration yielded higher *ksat* for larger return periods, while suction head clustered around ∼60–70 mm, and the initial deficit remained low (∼0.1), suggesting intensity-dependent compensation: as events intensify, the model increases effective conductivity to reproduce quicker throughflow and larger outflows. The resulting mean parameter set (e.g., *ksat* ≈ 61 mm/h) balances performance across scenarios but should be interpreted as an effective representation rather than a unique physical truth. Improving fit at low flows will likely require (1) better process representation (lateral inflow routing and along-slope variability), (2) tighter constraints on antecedent moisture states, and (3) higher-resolution observations to reduce timing and volume errors.

A limitation of this study arises from the calibration procedure, which relied on synthetic irrigation events under uniformly wet initial conditions (IMD = 0%). While this approach ensured controlled boundary conditions and reproducibility of observed outflows, it may not fully capture the variability in antecedent soil moisture that occurs under natural rainfall–drying cycles. In practice, grass swales undergo dynamic wetting and drying influenced by ET, shallow groundwater, and seasonal factors, which the calibration experiments did not explicitly reproduce. To mitigate this limitation, sensitivity analyses were conducted for a range of IMD values constrained by soil porosity, which confirmed the strong influence of antecedent moisture on overflow generation. These findings highlight the importance of interpreting the long-term simulations as indicative of relative trends, rather than absolute predictions, and suggest that future work should explicitly couple soil water balance models (including ET-driven recovery) with SWMM infiltration routines to better represent variable antecedent conditions.

5. CONCLUSIONS

A risk-based approach to estimating the risk of annual overflows from a GS was presented, and identified the influences of local climate, soil permeability, and physical characteristics of a specific GS on overflow occurrence. Three locations with different mechanisms of rainfall generation, frontal precipitation (in Gothenburg), convective rainfall (in Luleå), and convective and orographic precipitation (in Östersund), were included in the analysis. Results showed interannual variability in overflow risk, driven mainly by changes in total annual precipitation. Exceedance curves confirm that applying grass swales in regions with rainfall regimes similar to those analyzed in this article and low soil hydraulic conductivities (below the recommended value of 12 mm/h) will lead to facilities operating in failure mode during the entire period of analysis, unless mitigation measures are adopted. These findings confirm that locations with native soils of such low hydraulic conductivities are unsuitable for GS applications. While the results obtained suggest a minimum *ksat* of 31 mm/h to increase the time that the GS operates with an acceptable performance (50% in Gothenburg and 70% in Luleå), such infiltration rates are rarely found in native soils where grass swales are implemented. Additional design considerations should be explored to achieve acceptable operation, including building swales with greater cross-sectional areas, replacing native soils with engineered soils with higher hydraulic conductivities, or the addition of an underdrain in less permeable soils. Such design changes would require undertaking a benefit-cost analysis of the modified swale to ascertain its economic efficiency.

The results showed that, under the same soil conductivity and physical design characteristics, local climate – particularly total annual rainfall and ET – determines the occurrence of overflows. This effect was observed in Östersund modeled data, which is characterized by moderate annual rainfall (567 mm) and low-intensity events, making it the only location among those studied to operate with 100% acceptable performance for a *ksat* value of 31 mm/h. Exceedance curves indicate that acceptable performance is governed by local climate conditions and the presence of highly permeable soils. A characterization of climatic indicators, such as the occurrence of rainfall depths exceeding swale infiltration rates, should be incorporated into the estimation of swale retention capacities and the selection of GS physical properties, including cross-sectional area (e.g., width, length, and shape). Findings showed that climatic conditions less favorable for acceptable operation correspond to locations with an oceanic climate, characterized by frequent and consistent precipitation, well-distributed rainfall throughout the year (without marked dry or wet seasons).

The findings highlight the importance of identifying conditions that lead to a failed operation, and how such information could be incorporated into design modifications and verification of initial design parameters. Such findings are exacerbated in cold climate locations, where seasonal changes in soil hydraulic properties lead to a reduced hydrological performance during the winter period. Results from the present study suggest that when evaluating the acceptable operation of GSI, the focus should not be solely on the technical performance, but also on aligning the facility with broader management objectives, understanding risk tolerance, and considering the unique characteristics of the local site. Future work could apply climate projections to test whether current *ksat* thresholds remain effective under intensified rainfall. Coupling the 1D swale model with 2D inundation tools can link overflow volumes to flood extents and impacts, while multi-objective optimization and life-cycle cost–risk analysis can inform swale design, underdrain placement, and retrofit strategies for balanced performance and resilience.

ACKNOWLEDGEMENTS

This research was supported by Drizzle – Centre for Stormwater Management. The authors gratefully acknowledge the financial support provided by the VINNOVA (Swedish Governmental Agency for Innovation Systems) through the projects DRIZZLE – Centre for Stormwater Management (Grant No. 2022-03092).

DATA AVAILABILITY STATEMENT

All relevant data are included in the paper or its Supplementary Information.

CONFLICT OF INTEREST

The authors declare there is no conflict.

REFERENCES

Ahmed, F., Gulliver, J. S. & Nieber, J. L. (2015) Field infiltration measurements in grassed roadside drainage ditches: spatial and temporal variability, *Journal of Hydrology*, **530**, 604–611. https://doi.org/10.1016/j.jhydrol.2015.10.012.

Apel, H., Aronica, G. T., Kreibich, H. & Thieken, A. H. (2009) Flood risk analyses – how detailed do we need to be? *Natural Hazards*, **49** (1), 79–98. https://doi.org/10.1007/s11069-008-9277-8.

Bahrami, M., Roghani, B., Tscheikner-Gratl, F. & Rokstad, M. M. (2024) A deep dive into green infrastructure failures using fault tree analysis, *Water Research*, **257**, 121676. https://doi.org/10.1016/j.watres.2024.121676.

Ballard, B. W., Wilson, S., Udale-Clarke, H., Illman, S., Scott, T., Ashley, R. & Kellagher, R. (2015) *CIRIA SuDS Manual*, 5th edn. London: CIRIA.

Beryani, A., Goldstein, A., Al-Rubaei, A. M., Viklander, M., Hunt, W. F. & Blecken, G. T. (2021) Survey of the operational status of twenty-six urban stormwater biofilter facilities in Sweden, *Journal of Environmental Management*, **297** (March), 113375. https://doi.org/10.1016/j.jenvman.2021.113375.

Beryani, A., Flanagan, K., Viklander, M. & Blecken, G. T. (2023) Performance of a gross pollutant trap-biofilter and sand filter treatment train for the removal of organic micropollutants from highway stormwater (field study), *Science of the Total Environment*, **900**, 165734. https://doi.org/10.1016/j.scitotenv.2023.165734.

Brown, K., Hall, W. L. & Garvin, K. (2010) Preface. In: Brown, K., Hall, W. L. & Garvin, K. (eds.) *Sustainable Land Development and Restoration: Decision Consequence Analysis*, pp. xvii–xviii.

Cherqui, F., Szota, C., Fletcher, T. D. & Bertrand-Krajewski, J.-L. (2019) 'How to manage nature-based solution assets such as stormwater control measures? Available at: https://www.researchgate.net/publication/336888969

Dahlström, B. (2010) *Regnintensitet–en molnfysikalisk betraktelse*. Rapport Nr 2010-05. Stockholm: Svenskt Vatten Utveckling (SV-Utveckling), p. 46.

De Bruijn, K. M., Diermanse, F. L. M. & Beckers, J. V. L. (2014) An advanced method for flood risk analysis in river deltas, applied to societal flood fatality risk in The Netherlands, *Natural Hazards and Earth System Sciences*, **14** (10), 2767–2781. https://doi.org/10.5194/nhess-14-2767-2014.

Deletic, A. & Fletcher, T. D. (2006) Performance of grass filters used for stormwater treatment – a field and modelling study, *Journal of Hydrology*, **317** (3–4), 261–275. https://doi.org/10.1016/j.jhydrol.2005.05.021.

Ebrahimian, A., Sample-Lord, K., Wadzuk, B. & Traver, R. (2020) Temporal and spatial variation of infiltration in urban green infrastructure, *Hydrological Processes*, **34** (4), 1016–1034. https://doi.org/10.1002/hyp.13641.

Ekka, S. A., Hunt, W. F. & McLaughlin, R. A. (2024) Systematic evaluation of swale length, shape, and longitudinal slope with simulated highway runoff for better swale design, *Environmental Science and Pollution Research*, **32**, 22894–22916. https://doi.org/10.1007/s11356-024-35474-1.

Fletcher, T. D., Andrieu, H. & Hamel, P. (2013) Understanding, management and modelling of urban hydrology and its consequences for receiving waters: a state of the art, *Advances in Water Resources*, **51**, 261–279. https://doi.org/10.1016/j.advwatres.2012.09.001.

García-Serrana, M., Gulliver, J. S. & Nieber, J. L. (2017) Infiltration capacity of roadside filter strips with non-uniform overland flow, *Journal of Hydrology*, **545**, 451–462. https://doi.org/10.1016/j.jhydrol.2016.12.031.

Gironás, J., Roesner, L. A., Davis, J. & Rossman, L. A. (2009) *Storm Water Management Model Applications Manual*. Washington, DC: US EPA.

Gonzalez-Merchana, C., Barraud, S., Le Coustumer, S. & Fletcher, T. (2012) Monitoring of clogging evolution in the stormwater infiltration system and determinant factors, *European Journal of Environmental and Civil Engineering*, **16** (Suppl 1), s34–s47. https://doi.org/10.1080/19648189.2012.682457.

Green, W. H. & Ampt, G. A. (1911) Study on soil physics, *The Journal of Agricultural Science*, **4** (1), 1. doi:10.1017/S0021859600001441.

Hamouz, V., Pons, V., Sivertsen, E., Raspati, G. S., Bertrand-Krajewski, J.-L. & Muthanna, T. M. (2020) Detention-based green roofs for stormwater management under extreme precipitation due to climate change, *Blue-Green Systems*, **2** (1), 250–266. https://doi.org/10.2166/bgs.2020.101.

Hathaway, J. M., Brown, R. A., Fu, J. S. & Hunt, W. F. (2014) Bioretention function under climate change scenarios in North Carolina, USA, *Journal of Hydrology*, **519** (PA), 503–511. https://doi.org/10.1016/j.jhydrol.2014.07.037.

Hathaway, J. M., Bean, E. Z., Bernagros, J. T., Christian, D. P., Davani, H., Ebrahimian, A., Fairbaugh, C. M., Gulliver, J. S., McPhillips, L. E., Palino, G., Strecker, E. W., Tirpak, R. A., van Duin, B., Weinstein, N. & Winston, R. J. (2024) A synthesis of climate change impacts on stormwater management systems: designing for resiliency and future challenges, *Journal of Sustainable Water in the Built Environment*, **10** (2), 04023014. https://doi.org/10.1061/jswbay.sweng-533.

Hernebring, C. (2006) 10års-regnets återkomst, förr och nu - regndata för dimensionering/kontroll-beräkning av *VA-system i tätorter. VA.Forsk Rapport No.2006-04*.

International Standard Organization (2017) *ISO 1438: Hydrometry – Open Channel Flow Measurement Using Thin-Plate Weirs*, 3rd edn. Geneva, Switzerland: ISO, p. 60.

Johansson, B. & Chen, D. (2003) The influence of wind and topography on precipitation distribution in Sweden: statistical analysis and modelling, *International Journal of Climatology: A Journal of the Royal Meteorological Society*, **23**, 1523–1535. https://doi.org/10.1002/joc.951.

Kanso, T., Tedoldi, D., Gromaire, M. C., Ramier, D., Saad, M. & Chebbo, G. (2018) Horizontal and vertical variability of soil hydraulic properties in roadside sustainable drainage systems (SuDS) – nature and implications for hydrological performance evaluation, *Water (Switzerland)*, **10** (8), 987. https://doi.org/10.3390/w10080987.

Kindsvater, C. E. & Carter, R. W. C. (1957) Discharge characteristics of rectangular thin-plate weirs, *Journal of the Hydraulics Division, Proceedings of the American Society of Civil Engineers*, **83** (6), 1453.

Köppen, W. & Geiger, R. (1936) *Handbuch der Klimatologie in Fünf Bänden Das Geographische System der Klimate*. Berlin: Norntraeger Science Publisher. Available at: www.borntraeger-cramer.com.

Korving, H., van Noortwijk, J. M., van Gelder, P. H. A. J. M. & Clemens, F. H. L. R. (2009) Risk-based design of sewer system rehabilitation, *Structure and Infrastructure Engineering*, **5** (3), 215–227. https://doi.org/10.1080/15732470601114299.

Langeveld, J. G., Cherqui, F., Tscheikner-Gratl, F., Muthanna, T. M., Juarez, M. F. D., Leitão, J. P., Roghani, B., Kerres, K., do Céu Almeida, M., Werey, C. & Rulleau, B. (2022) Asset management for blue-green infrastructures: a scoping review, *Blue-Green Systems*, **4** (2), 272–290. https://doi.org/10.2166/bgs.2022.019.

Le Coustumer, S., Fletcher, T. D., Deletic, A., Barraud, S. & Lewis, J. F. (2009) Hydraulic performance of biofilter systems for stormwater management: influences of design and operation, *Journal of Hydrology*, **376** (1–2), 16–23. https://doi.org/10.1016/j.jhydrol.2009.07.012.

Leroy, M. C., Portet-Koltalo, F., Legras, M., Lederf, F., Moncond'huy, V., Polaert, I. & Marcotte, S. (2016) Performance of vegetated swales for improving road runoff quality in a moderate traffic urban area, *Science of the Total Environment*, **566–567**, 113–121. https://doi.org/10.1016/j.scitotenv.2016.05.027.

Lewellyn, C. & Wadzuk, B. (2019) Risk-based methodology for evaluation of bioinfiltration design and performance, *Journal of Sustainable Water in the Built Environment*, **5** (1), 04018014. https://doi.org/10.1061/jswbay.0000869.

Lewellyn, C., Lyons, C. E., Traver, R. G. & Wadzuk, B. M. (2016) Evaluation of seasonal and large storm runoff volume capture of an infiltration green infrastructure system, *Journal of Hydrologic Engineering*, **21** (1), 04015047. https://doi.org/10.1061/(asce)he.1943-5584.0001257.

Lhamidi, K., El Khattabi, J., Nguyen, H. D. & Aljer, A. (2024) Hydrological performance assessment of low-impact development practices: a vegetated swale case study, *Water (Switzerland)*, **16** (14), 2018. https://doi.org/10.3390/w16142018.

Lindholm, O., Endresen, S., Thorolfsson, S., Sægrov, S., Jakobsen, G. & Aaby, L. (2008) *Veiledning i klimatilpasset overvannshåndtering*. Oslo: Norsk Vann Rapport.

Mantilla, I., Flanagan, K., Broekhuizen, I., Merete Muthanna, T., Marsalek, J. C. & Viklander, M. (2024) Retrofit of grass swales with outflow controls for enhancing drainage capacity, *Journal of Hydrology*, **639**, 131637. https://doi.org/10.1016/j.jhydrol.2024.131637.

Mantilla, I., Muthanna, T. M., Marsalek, J. & Viklander, M. (2025) Assessing spatial and temporal variability of grass swale infiltration in shallow groundwater conditions, *Journal of Environmental Management*, **380**, 124977. https://doi.org/10.1016/j.jenvman.2025.124977.

MDE (2009) *2000 Maryland Stormwater Design Manual Volumes I & II*, Water, 4. Baltimore, MD: Maryland Department of the Environment.

Mens, M. J. P., Klijn, F., de Bruijn, K. M. & van Beek, E. (2011) The meaning of system robustness for flood risk management, *Environmental Science and Policy*, **14** (8), 1121–1131. https://doi.org/10.1016/j.envsci.2011.08.003.

MPCA (2005) *The Minnesota Stormwater Manual*. St. Paul, MN: Minnesota Pollution Control Agency.

Park, J., Seager, T. P., Rao, P. S. C., Convertino, M. & Linkov, I. (2013) Integrating risk and resilience approaches to catastrophe management in engineering systems, *Risk Analysis*, **33** (3), 356–367. https://doi.org/10.1111/j.1539-6924.2012.01885.x.

Paus, K. H., Muthanna, T. M. & Braskerud, B. C. (2016) The hydrological performance of bioretention cells in regions with cold climates: Seasonal variation and implications for design, *Hydrology Research*, **47** (2), 291–304. https://doi.org/10.2166/nh.2015.084.

Paus, K. H. (2018) Forslag til dimensjonerende verdier for trinn 1 i Norsk Vann sin tre-trinns strategi for håndtering av overvann, *Vannforeningen*, **53** (1), 66–77.

Pons, V., Benestad, R., Sivertsen, E., Muthanna, T. M. & Bertrand-Krajewski, J. L. (2022a) Forecasting green roof detention performance by temporal downscaling of precipitation time-series projections, *Hydrology and Earth System Sciences*, **26** (11), 2855–2874. https://doi.org/10.5194/hess-26-2855-2022.

Pons, V., Muthanna, T. M., Sivertsen, E. & Bertrand-Krajewski, J. L. (2022b) Revising green roof design methods with downscaling model of rainfall time series, *Water Science and Technology*, **85** (5), 1363–1371. https://doi.org/10.2166/wst.2022.023.

Rawls, W. J., Brakensiek, C. L. & Saxton, K. E. (1982) Estimation of soil water properties, *Transactions – American Society of Agricultural Engineers*, **25** (5), 1316–1320. https://doi.org/10.13031/2013.33720.

Rawls, W. J., Brakensiek, D. L. & Miller, N. (1983) Green-ampt infiltration parameters from soils data, *Journal of Hydraulic Engineering*, **109** (1), 62–70. https://doi.org/10.1061/(asce)0733-9429(1983)109:1(62).

Rodriguez, M., Fu, G., Butler, D., Yuan, Z. & Sharma, K. (2021) Exploring the spatial impact of green infrastructure on urban drainage resilience, *Water (Switzerland)*, **13** (13), 1789. https://doi.org/10.3390/w13131789.

Rodriguez, M., Fu, G., Butler, D., Yuan, Z. & Cook, L. (2023) Global resilience analysis of combined sewer systems under continuous hydrologic simulation, *Journal of Environmental Management*, **344**, 118607. https://doi.org/10.1016/j.jenvman.2023.118607.

Rossman, L. A. (2015) *Storm Water Management Model User's Manual*. Version II. Environ Prot Technol Ser EPA, 670/2-75–017. Washington, DC: US EPA.

Rossman, L. A. (2016) *Storm Water Management Model Reference Manual Volume I-Hydrology*. Washington, DC: US EPA.

Rossman, L. A. & Huber, W. C. (2016) *Storm Water Management Model Reference Manual Volume I – Hydrology (Revised) (EPA/600/R-15/162A), Vol. I (January)*. Washington, DC: U.S. Environmental Protection Agency, p. 231.

Rujner, H., Leonhardt, G., Marsalek, J., Perttu, A. M. & Viklander, M. (2018) The effects of initial soil moisture conditions on swale flow hydrographs, *Hydrological Processes*, **32** (5), 644–654. https://doi.org/10.1002/hyp.11446.

Sage, J., Berthier, E. & Gromaire, M. C. (2015) Stormwater management criteria for on-site pollution control: a comparative assessment of international practices, *Environmental Management*, **56** (1), 66–80. https://doi.org/10.1007/s00267-015-0485-1.

Skivington, P. (1997) *Risk Assessment for Water Quality Management: Final Report to the Water Research Commission*. Marshaltown: WRC.

Sohn, W., Brody, S. D., Kim, J. H. & Li, M. H. (2020) How effective are drainage systems in mitigating flood losses? *Cities*, **107** (November 2019), 102917. https://doi.org/10.1016/j.cities.2020.102917.

Staccione, A., Essenfelder, A. H., Bagli, S. & Mysiak, J. (2024) Connected urban green spaces for pluvial flood risk reduction in the Metropolitan area of Milan, *Sustainable Cities and Society*, **104**, 105288. https://doi.org/10.1016/j.scs.2024.105288.

Svenskt Vatten (SV) (2016) *P110: avledning av dag-, drän- och spillvatten. Funktionskrav, hydraulisk dimensionering och utformning av allmänna avloppssystem*. Stockholm: Svenskt Vatten Utveckling (SV-Utveckling).

Tirpak, R. A., Hathaway, J. M., Khojandi, A., Weathers, M. & Epps, T. H. (2021a) Building resiliency to climate change uncertainty through bioretention design modifications, *Journal of Environmental Management*, **287** (March), 112300. https://doi.org/10.1016/j.jenvman.2021.112300.

Tirpak, R. A., Hathaway, J. M., Khojandi, A., Weathers, M. & Epps, T. H. (2021b) Building resiliency to climate change uncertainty through bioretention design modifications, *Journal of Environmental Management*, **287** (February), 112300. https://doi.org/10.1016/j.jenvman.2021.112300.

UDFCD (2016) *Urban Storm Drainage. Criteria Manual. Urban, 1*. Denver, CO: Urban Drainage and Flood Control District.

UNEP (2023) *Climate Change 2023: Synthesis Report*. Geneva: UNEP – UN Environment Programme, pp. 35–115.

US EPA (2021) *(2021) Stormwater Best Management Practice Grassed Swales Minimum Measure: Post Construction Stormwater Management in New Development and Redevelopment Subcategory: Infiltration*. Washington, DC: US EPA. https://www.epa.gov/npdes.

Vorogushyn, S., Bates, P. D., Debruijn, K., Castellarin, A., Kreibich, H., Priest, S., Schroter, K., Bagli, S., Bloschl, G., Domeneghetti, A., Gouldby, B., Klijn, F., Lammersen, R., Neal, J. C., Ridder, N., Terink, W., Viavattene, C., Viglione, A., Zanardo, S. & Merz, B. (2018) Evolutionary leap in large-scale flood risk assessment needed, *Wiley Interdisciplinary Reviews: Water*, **5** (2), e1266. https://doi.org/10.1002/WAT2.1266.

Weathers, M., Hathaway, J. M., Tirpak, R. A. & Khojandi, A. (2023) Evaluating the impact of climate change on future bioretention performance across the contiguous United States, *Journal of Hydrology*, **616** (October 2022), 128771. https://doi.org/10.1016/j.jhydrol.2022.128771.

Winston, R. J., Dorsey, J. D. & Hunt, W. F. (2016) Quantifying volume reduction and peak flow mitigation for three bioretention cells in clay soils in northeast Ohio, *Science of the Total Environment*, **553**, 83–95. https://doi.org/10.1016/j.scitotenv.2016.02.081.

Winston, R. J., Anderson, A. R. & Hunt, W. F. (2017) Modeling sediment reduction in grass swales and vegetated filter strips using particle settling theory, *Journal of Environmental Engineering*, **143** (1), 1–11. https://doi.org/10.1061/(asce)ee.1943-7870.0001162.

Yen, B. C. (2002) Open channel flow resistance, *Journal of Hydraulic Engineering*, **128** (1), 20–39. https://doi.org/10.1061/(asce)0733-9429(2002)128:1(20).

First received 31 March 2025; accepted in revised form 27 October 2025. Available online 11 November 2025